Stochastic Modelling of Solidification Grain Structures.

Charles-André Gandin, Ch. Charbon, Michel Rappaz

ISIJ International, Vol. 35 (1995), No. 6, pp. 651–657

Stochastic Modelling of Solidification Grain Structures

Ch.-A. GANDIN, Ch. CHARBON and M. RAPPAZ

Ecole Polytechnique Fédérale de Lausanne, Laboratoire de Métallurgie Physique MX-G, CH-1015 Lausanne, Switzerland.

(*Received on January 17, 1995; accepted in final form on March 10, 1995*)

Stochastic models have been developed for the simulation of grain structure formation during the solidification of metallic alloys. Nucleation is assumed to occur randomly in space according to a prescribed distribution of nucleation sites. For dendritic alloys, the hypothesis of a random orientation of the ⟨100⟩ crystallographic directions of the new nuclei is also made. A cellular automaton (CA) and an interface-tracking technique are used to follow the growth-impingement of dendritic and eutectic grains, respectively. The influence of the local thermal conditions, namely the thermal gradient and the velocity of the isotherm, and of the nucleation parameters on the resulting grain structures is assessed. In particular, it is shown that the asymmetry of the grains along the thermal gradient is an increasing function of the thermal gradient and nucleation undercooling and a decreasing function of the velocity and grain density. The presence of the outer equiaxed zone and the transition from columnar to equiaxed microstructures can also be explained using such models.

KEY WORDS: solidification; dendritic and eutectic grain structures; stochastic modelling; cellular automaton.

1. Introduction

The control of grain structure is essential in many solidification processes. In most cases, fine equiaxed grains are required in order to obtain homogeneous and isotropic mechanical properties. This is usually achieved by the addition of inoculant particles to the molten metal or by the fragmentation of dendrites through mechanical- or electromagnetic-induced shearing of the melt. However, other applications, such as superalloy turbine blades, require directional properties in which case columnar structures must be produced by directional solidification. In order to control the microstructures in casting, it is necessary to master both the process parameters and the microscopic phenomena governing the nucleation and growth of grains. In this field, simulation can be a very powerful tool as will be demonstrated in this paper.

Substantial recent progress has been made in the simulation of solidification processes for several reasons: (1) an improved knowledge of the basic mechanisms governing the development of microstructures and defects[1–3]; (2) the development of sophisticated numerical techniques and (3) the advent of very powerful workstations. However, it is interesting to note that most of the developments in this area have been made either at the macroscopic scale of the process (*i.e.*, resolution of the continuity equations governing mass, energy, momentum and solute transports) or at the microscopic level of the dendrite tips or eutectic lamellae. The goal of micro-macroscopic models of solidification is to combine these two scales in a single approach in order to predict the grain structures and defects in a given process.[4]

Deterministic models have been first developed for the description of the nucleation, growth and impingement of equiaxed grains in solidification processes. A review of these models has been made in Ref. 4). However, these models suffer from several limitations: (1) the grains are assumed to remain spherical even in a strong thermal gradient; (2) columnar structures and thus the columnar-to-equiaxed transition (CET) are usually not accounted for; (3) the competition occuring among grains belonging to the columnar zone and (4) the associated evolution of their crystallographic texture are not described at all; (5) simulated micrographs cannot be produced using such models.

For the reasons mentioned above, the simulation of grain structure formation in solidification processes has been approached using *stochastic methods*. The first model developed by Brown and Spittle[5] was based upon a Monte Carlo (MC) method similar to that previously described by Anderson *et al.*[6] for the prediction of grain growth in solids. Zhu and Smith modified this technique and implemented it in a Finite Difference (FD) calculation of heat flow.[7] Although the MC method has proved to be successful in producing grain structures which resemble those encountered in real castings, it lacks the physical mechanisms associated with dendritic or eutectic growth.[3] In particular, it does not account for the growth kinetics of dendrite tips (or eutectic front) and for the preferential growth directions of the dendrites. For those reasons, *physically-based stochastic models* were developed over the past three

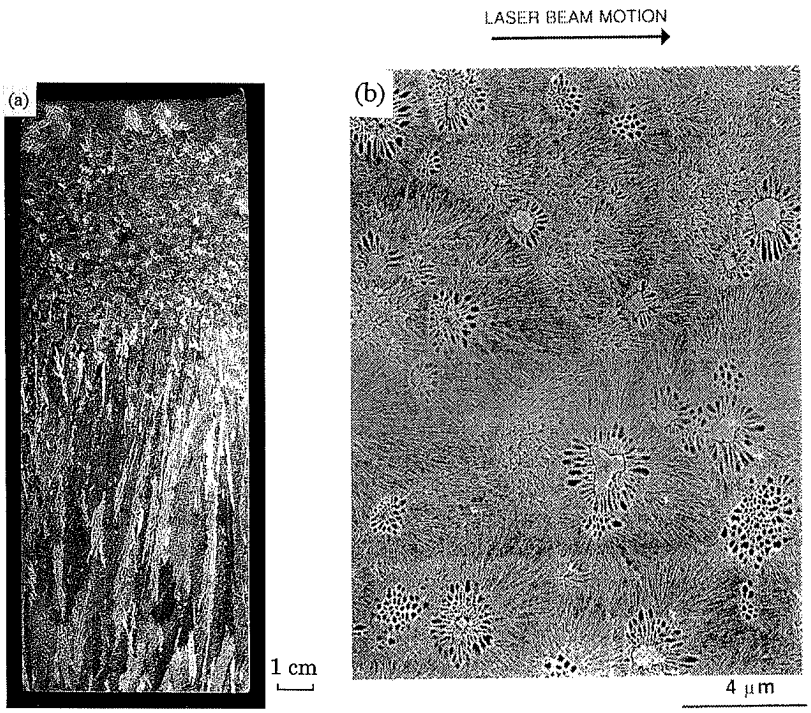

Fig. 1.
Experimental section micrographs of: (a) an Al–7wt%Si ingot directionally solidified in a pre-heated ceramic mould over a copper-chill plate (after Ref. 9)); (b) an Al–26wt%Si alloy remelted by a moving high-power laser beam (after Ref. 13)).

years for the simulation of eutectic[8] and dendritic[9] grain structure formation under various solidification conditions. The purpose of the present contribution is not to detail these models but rather to show a few examples demonstrating their capabilities.

2. Experimental Observations

Figure 1(a) shows the longitudinal section of an aluminium–7wt% silicon alloy directionally solidified over a copper chill plate. The details of the experiment used to produce such an ingot are described in Ref. 10). In order to eliminate any convection associated with pouring, the liquid metal and mould were initially maintained at a constant temperature (39°C superheat), before a water-cooled copper chill was applied to the bottom of the mould. The lateral sides of the mould were made from an insulated ceramic material so that the isotherms remained horizontal during the entire solidification process. Furthermore, considering the alloy components and the experimental configuration, thermo-solutal convection was eliminated. Grains could only form by heterogeneous nucleation over the bottom plate or in the bulk of the liquid melt and not by dendrite fragmentation.[11] Four zones can be seen in Fig. 1(a): (1) fine grains (outer equiaxed region) very close to the bottom surface of the casting; (2) long columnar grains growing from the outer equiaxed region; (3) grains of elongated shape at the mid-height of the casting, but much shorter and narrower than the columnar grains; and finally (4) an "inner" equiaxed region near the top of the casting*.

The formation of the outer equiaxed zone and the selection of columnar grains from this zone have not been extensively analysed in the literature, whereas several mechanisms have been invoked for the transition from the columnar to the equiaxed zones (CET).[9] Under the present experimental conditions, however, the only mechanism that can be active for the CET is the heterogeneous nucleation of grains in an undercooled liquid ahead of the growing columnar front.[12] As may be seen in Fig. 1(a), the CET is not abrupt: the long columnar grains issued from the bottom part are progressively outgrown by grains nucleating in the bulk of the liquid but still growing in a thermal gradient (zone of elongated grains). These grains become truely equiaxed (almost isotropic shape) in the upper part of Fig. 1(a) when the thermal gradient is drastically reduced. It is clear that deterministic models of solidification are not able to predict the grain selection which operates in the columnar zone and the gradual change in the morphology of the grains which nucleate in the bulk of the liquid (zones (3) and (4) containing elongated and equiaxed grains).

The formation of "equiaxed" eutectic grains in a thermal gradient is illustrated in **Fig. 1(b)** for an Al–26wt%Si alloy remelted by laser.[13] A high power CO_2 laser beam source (1.5 kW, focus diameter 0.34 mm) was moved at a velocity, $v = 0.1$ m/s, over the workpiece. The micrograph shown in Fig. 1(b) corresponds to a longitudinal section taken near to the top free surface of the material. Under such conditions, it has been shown that the actual velocity of the eutectic isotherm near the top surface is close to that of the velocity of the moving laser beam and that the thermal gradient is of the order of 10^6°C/m.[8] As can be seen, the microstructure clearly

* Equiaxed grains are usually found at the centre of conventional castings. Being surrounded by columnar grains, they form the "inner" equiaxed zone. In the present situation (adiabatic boundary condition at the top surface of the casting), this zone appears in the upper half of Fig. 1(a).

consists of grains which have nucleated in the bulk of the liquid. In this micrograph, the centre of nucleation of some of the grains is revealed by the presence of a primary silicon crystal. The silicon forms first in this hypereutectic alloy and is surrounded by a cellular α-aluminium structure and then by the eutectic grain morphology.

As clearly revealed in Fig. 1(b), the final shape of the grains deviates from the spherical geometry assumed in deterministic models. The grains seem to grow preferentially in the direction opposite to the heat flow direction (the heat flow is opposite to the travel direction of the laser beam shown by an arrow at the top of the micrograph). As will be shown in the next sections, this effect is associated with the impingement of grains nucleating and growing in a thermal gradient. It can only be accounted for by stochastic models of solidification.

In order to model the grain structures shown in Fig. 1, it is necessary to simulate both the nucleation and growth of grains. The next section presents the algorithms used for the simulation of the growth of a single grain for both dendritic and eutectic alloys. These algorithms will be coupled then with a stochastic nucleation procedure in order to simulate a complete micrograph.

3. Growth of a Single Grain

3.1. Dendritic Grain

The growth of a single two-dimensional dendritic grain has been modelled using a Cellular Automaton (CA) algorithm.[9] In this approach, the square solidifying domain is divided into a large number of regular square cells. The temperature at each cell location is assumed to vary according to fixed thermal gradient, G, and cooling rate, $\dot{T}$, (*i.e.*, Bridgman conditions). One grain is nucleated at the centre of the grid at a predetermined nucleation undercooling, ΔT_n. The crystallographic orientation of the grain is set to a prescribed value, one of the $\langle 100 \rangle$ directions being considered perpendicular to the plane used for the simulation (*i.e.*, two-dimensional growth situation). Under isothermal conditions (*i.e.*, $G=0$), the grain is assumed to grow as a square whose diagonals correspond to the two other preferential $\langle 100 \rangle$ growth directions of the dendrites.[9] This square outlines the envelope of the dendrite arms. The velocity of these dendrite tips and arms, v, is an increasing function of the local undercooling, ΔT. In the present case, the model of Kurz, Giovanola and Trivedi (KGT)[14] has been used to deduce the $v(\Delta T)$ relationship. The CA growth algorithm can be then summarised as follows: a small square is grown at the nucleation cell location with the prescribed orientation of the $\langle 100 \rangle$ directions and the velocity $v(\Delta T(t))$. At a given time, this square reaches the position of the four nearest-neighbour cells. From that instant, the central cell is no longer considered and the dendritic network is grown similarly in each of these cells using the local undercooling at the corresponding cell location. Thus, the dendritic network is propagated from cells to cells. Special care must be taken in order to preserve the original misorientation of the grain. The details of the CA algorithm are given in Ref. 9).

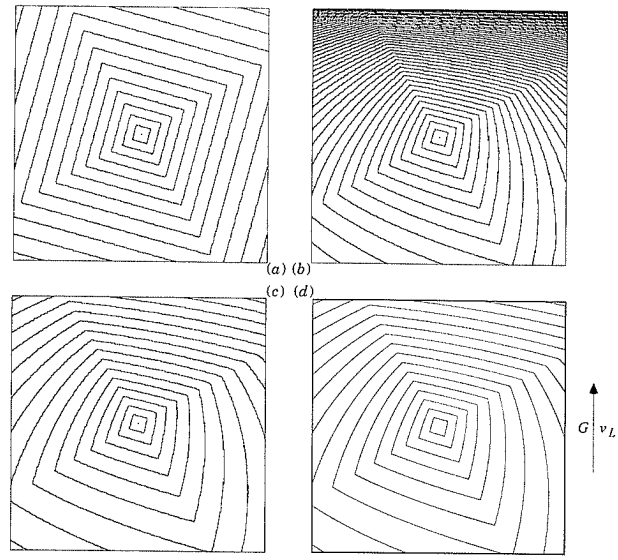

Fig. 2. Growth of an isolated dendritic grain under various thermal conditions: (a) $G=0$°C/m, $\dot{T}=-0.1$°C/s; (b) $G=250$°C/m, $\dot{T}=0$°C/s; (c) $G=250$°C/m, $\dot{T}=-0.1$ °C/s. The various dendrite interface positions have been drawn every 1 sec. The shapes of the grain shown in (d) have been obtained from an analytical integration of the dendrite growth kinetics ($v=10^{-4}\cdot\Delta T^2\,\mathrm{m\cdot s^{-1}}$) under the thermal conditions of case (c). The grain has been nucleated at time $t=0$ s with an initial undercooling $\Delta T_n=2$°C. The size of the square solidifying domain is 1 cm × 1 cm.

Figure 2 shows the simulated growth of a single dendritic grain under various thermal environments. The [100] orientation of the grain is at +30 deg with respect to the horizontal and the initial nucleation undercooling is set to 2°C. The grain interface is plotted every 1 sec after the nucleation event. In **Fig. 2(a)**, the thermal gradient was set to zero and $\dot{T}=-0.1$°C/s. As can be seen, the CA algorithm does indeed preserve the original misorientation of the nucleus. As the uniform undercooling increases with time, the interface accelerates and thus the spacing between the grain envelope positions becomes larger. The zigzag interfaces of the grain are due to the size of the cells (25 μm) used in the computations. **Figure 2(b)** corresponds to $G=250$°C/m and $\dot{T}=0$°C/s (*i.e.*, growth in a unidirectional thermal gradient with a zero velocity of the isotherms). As the gradient is vertical, the portion of the grain located above the nucleation cell tends asymptotically to the position of the liquidus isotherm (upper boundary of the square domain). Since the undercooling for this part of the grain envelope decreases, the velocity also decreases and the interface positions become closer as time proceeds. On the contrary, the portion of the grain located below the nucleation cell becomes more undercooled and thus grows faster. This demonstrates that an isolated grain grows faster in the direction of the heat flow.

In **Fig. 2(c)**, the grain grows in the same gradient $G=$ 250°C/m but with a cooling rate, $\dot{T}=-0.1$°C/s (*i.e.*, speed of the horizontally moving liquidus isotherms, v_L, equal to 400 μm/s). Under such conditions, the portion of the

grain located above the nucleation cell tends again to align with the moving liquidus isotherm whereas the bottom portion grows in an increasingly undercooled liquid. The grain morphology obtained under such conditions with the CA can be compared with the analytical solution shown in **Fig. 2(d)**. This solution is similar to that obtained for the growth of eutectic grains in a thermal gradient[8] but considering the anisotropic growth of the dendrites[15] : for the two upper $\langle 100 \rangle$ directions growing in the direction of the thermal gradient, this solution is given by a hyperbolic tangent of the undercooling whereas, for the two directions growing downward, the solution is proportional to the tangent of the undercooling. As a result, the growth toward the heat flow direction is "catastrophic", *i.e.*, the velocity of the grain can become infinite. As will be shown, this portion of the grain is usually limited by other grains which have previously nucleated and grown. In the upper direction, the asymptotic limit of the growth is given by the speed of the liquidus isotherm.

3.2. Eutectic Grain

For eutectic grains, the normal velocity of the interface is assumed to obey the model of Jackson and Hunt[16] (*i.e.*, $v = A \cdot \Delta T^2$ where A is a growth constant function of the alloy). In this case, an interface tracking method has been used to calculate the evolution of a single grain. This method is described in details in Ref. 8). From the centre of nucleation, several radial directions are chosen (see **Fig. 3**). The position of the grain interface is then described by a set of radii, $r(\theta_i, t)$, where θ_i are equally spaced angles used to track the interface (*i.e.*, "shooting directions"). The radial velocity is then given by[8]:

$$\frac{dr}{dt} = A \cdot [\Delta T(r)]^2 \sqrt{1 + \left[\frac{r'}{r}\right]^2} \quad \text{.....(1)}$$

where r' is the derivative $dr/d\theta$. This derivative can be calculated numerically for each time step from the actual position of the interface, and the new position of the shooting directions, $r(\theta_i, t+\Delta t)$, can be found. The undercooling, $\Delta T(r)$, at each corresponding radial distance is used in this computation.

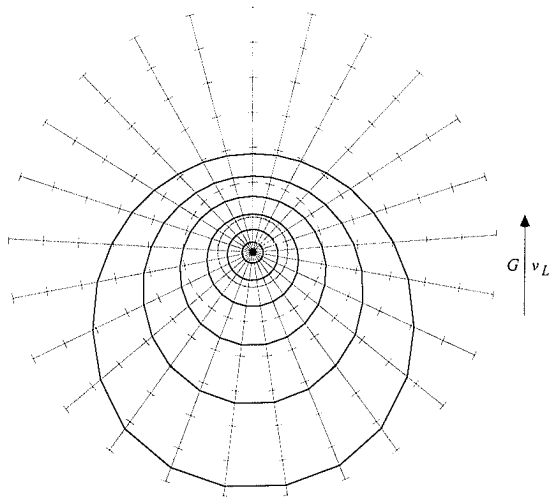

Fig. 3. Growth of an isolated eutectic grain in a thermal gradient $G = 2 \cdot 10^6$°C/m at a cooling rate $\dot{T} = -2 \cdot 10^5$ °C/s (*i.e.*, $v = 0.1$ m/s). The various grain interface positions have been drawn every 200 μs and the tick spacing corresponds to 5 μm. The grain has been nucleated at time $t = 0$ s with an initial undercooling $\Delta T_n = 50$°C.

The result of such a calculation is shown in Fig. 3 for a eutectic grain growing under thermal conditions similar to those found in laser remelting (see Fig. 1(b)). The gradient G and cooling rate $\dot{T}$ are set to $2 \cdot 10^6$°C/m and $-2 \cdot 10^5$°C/s, respectively (*i.e.*, speed of the horizontally moving eutectic isotherm, v_E, equal to 0.1 m/s). The nucleation undercooling is equal to 50°C and the position of the grain interface has been plotted every 200 μs. As for the dendritic grain, it can be seen that the portion of the grain opposite to the thermal gradient grows fastest because it is most undercooled. In the direction of the thermal gradient, the grain tends to follow the eutectic isotherm which moves upwards.

In the next section, it is shown how these single grain growth models can be used to describe the nucleation, growth and impingement of a family of grains.

4. Modelling of Grain Structures

4.1. Modelling of Nucleation and Growth

In most specimens, the nucleation of the grains occurs heterogeneously on some nucleation sites, which are assumed to be randomly distributed within the volume of the liquid. Some nuclei may also form at the surface of a mould but the emphasis here is placed upon bulk nucleation. The nucleation approach which is adopted here is similar to that used in deterministic models.[4] At small undercooling, nucleation occurs almost instantaneously on each family of nucleation sites. Each family is described by a density of sites per unit volume and by a potency, *i.e.*, by a critical undercooling at which nucleation occurs on these sites. Accordingly, the density of nuclei, $n(\Delta T)$, which have formed within the melt at a given undercooling, ΔT, is given by:

$$n(\Delta T) = \int_0^{\Delta T} p(\Delta T') \cdot d(\Delta T') \quad \text{.....(2)}$$

where $p(\Delta T)$ is the distribution of nucleation site families, assumed to be a continuous function in Eq. (2). This distribution must be determined *a posteriori* from experimental measurements performed under various cooling conditions.[4]

In a stochastic model, these nucleation sites are randomly distributed within the melt. For that purpose, a total of N square cells in the CA grid are used to map the surface, S, of the specimen (the volume in three dimensions). Each cell has a dimension $l = \sqrt{S/N}$. The number of sites, δN_n, which can become active in the undercooling interval $[\Delta T_n, \Delta T_n + \delta(\Delta T)]$ is given by $p(\Delta T_n) \cdot \delta(\Delta T) \cdot S$. Therefore, δN_n cells are randomly chosen among the total number of cells, $N (N \gg \delta N_n)$. The prescribed undercooling, ΔT_n, is then attributed to these "nucleation cells". The procedure is repeated before the start of the solidification computation for a continuous undercooling range, extending from zero to a maximum undercooling which will be attained during the calculation. If a nucleation cell is selected several times

during this procedure, only the minimum undercooling is kept since it is assumed that the less-potent nucleation sites (larger nucleation undercooling) will be trapped by the grain formed at higher temperature on the more-potent site.

Once the nucleation cells have been defined, the time stepping calculation for the simulation of the solidification of the specimen can be started. The temperature at each cell location is deduced according to two different methods: for eutectics, the thermal history is assumed to correspond as before to an ideal Bridgman situation (constant cooling rate and gradient) whereas, for dendritic alloys, it is calculated using a finite element (FE) heat flow code.[17] In the second case, the FE mesh is much coarser than the CA grid and the FE computation is coupled with the latent heat released at the cell location. The details of this CA-FE coupling are given in Ref. 9). If the local undercooling at a nucleation cell location becomes larger than its prescribed nucleation undercooling (*i.e.*, $\Delta T > \Delta T_n$) and the cell is still liquid, then a new grain is formed. For dendritic alloys, the crystallographic orientation of this grain is selected randomly among a number of orientation classes. The CA algorithm or the interface tracking methods are then used to follow the evolution of the grains of dendritic or eutectic alloys, respectively. In the latter case, the grid defined for the nucleation algorithm is used for the visualisation of the grains: all the cells falling within the envelope of a eutectic grain are attributed to this grain. For dendritic specimens, the same CA grid is used for the choice of the nucleation cells and for the growth algorithm.

4.2. Columnar to Equiaxed Transition

Figure 4 shows the results of the CA-FE model applied to the one-dimensional Al–7wt%Si casting of Fig. 1(a). The boundary conditions at the bottom surface of the ingot were deduced by an inverse method[18] using the temperatures measured at several locations in the copper chill. The thermal conductivity, latent heat and specific heat of this alloy were taken from Ref. 19). The growth kinetics of the dendrite tips was calculated using the KGT model and the thermophysical properties given also in Ref. 19). The $v(\Delta T)$ relationship obtained for this alloy was then fitted to the polynomial law:

$$v = a_2 \cdot \Delta T^2 + a_3 \cdot \Delta T^3 \quad \text{.....(3)}$$

with $a_2 = 2.70 \cdot 10^{-6}\,\mathrm{m \cdot s^{-1} \cdot °C^{-2}}$ and $a_3 = 1.19 \cdot 10^{-6}\,\mathrm{m \cdot s^{-1} \cdot °C^{-2}}$. The only parameters which were then varied are those associated with the nucleation in the bulk of the liquid. In this case, the nucleation site distribution, $p(\Delta T)$, was assumed to be given by a Gaussian law:

$$p(\Delta T) = \frac{n_{\max}}{\sqrt{2\pi}\,\Delta T_\sigma} \exp\left\{ -\left[\frac{\Delta T - \Delta T_N}{\sqrt{2}\,\Delta T_\sigma} \right]^2 \right\} \quad \text{....(4)}$$

$n_{\max}$ is the maximum density of grains that can form in the melt. It was set to $4.7 \cdot 10^{10}\,\mathrm{m^{-3}}$. The standard deviation of the distribution, ΔT_σ, was also fixed to a constant value of 0.5°C. The only parameter that was changed for the three cases shown in Fig. 4 was the centre of the distribution, ΔT_N. It was set to 4.5, 5 and 5.5°C for the cases (a), (b) and (c), respectively. As ΔT_σ is quite small, the nucleation can be said to occur at ΔT_N.

As shown in Fig. 4, a very small change of ΔT_N strongly affects the resulting microstructure. In **Fig. 4(a)**, the structure is equiaxed throughout almost the entire casting. The grains are very fine and nearly equiaxed near the bottom surface. They become slightly elongated at about 2 cm from the chill surface and then again equiaxed above 4 cm. The grain structure becomes much coarser near the top surface of the ingot. The same features are much more pronounced in **Fig. 4(b)**. In particular, the zone of elongated grains becomes broader. Some grain competition occurs within this zone, *i.e.*, the grains which

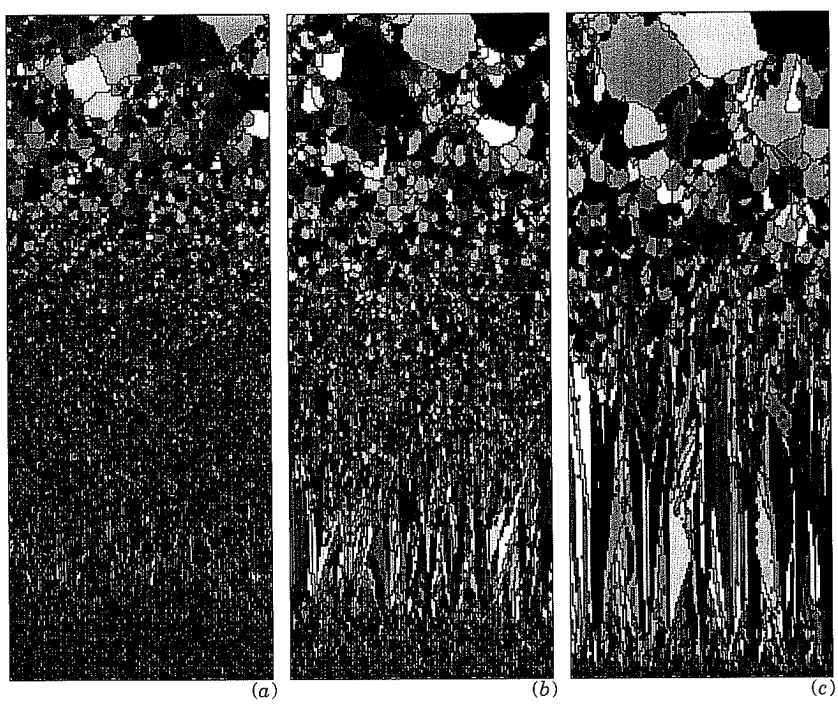

Fig. 4.
Two-dimensional grain structures calculated with the CAFE model for an Al–7wt%Si alloy directionally solidified under the same thermal conditions as the ingot shown in Fig. 1(a). The three cases (a–c) correspond to slightly different mean nucleation undercoolings, ΔT_N: 4.5°C (a), 5°C (b) and 5.5°C (c). ($n_{\max} = 4.7 \cdot 10^{10}\,\mathrm{m^{-3}}$, $\Delta T_\sigma = 0.5$°C). The height of the simulation domain is equal to that of the ingot shown in Fig. 1(a).

have one of their ⟨100⟩ directions best aligned with the vertical thermal gradient tend to eliminate those of poorer orientation. The grains just above this zone are coarser and slightly more elongated in Fig. 4(b) compared to the same zone in Fig. 4(a). Finally, in **Fig. 4(c)**, the zone of elongated grains can now be called "columnar" because it extends over almost half of the ingot. Within this zone, some spurious grains have nucleated in the bulk of the liquid but were quickly outgrown by the long columnar grains. The three other grain morphologies seen above and below the columnar zone are in close agreement with the experimental results shown in Fig. 1(a): outer equiaxed zone at the bottom, elongated grains above and finally, coarse equiaxed grains at the top of the ingot.

4.3. Asymmetry of Grains

Rappaz *et al.*[8] have shown that the asymmetry factor of eutectic grains formed by heterogenous nucleation in the bulk of the liquid is an increasing function of the thermal gradient and of the nucleation undercooling, whereas it is a decreasing function of the velocity of the isotherm and of the grain density. In Fig. 4, the same trend is observed in the three cases where the average undercooling is increased (*i.e.*, the grains are most elongated in (c) for which ΔT_N is largest). The range of ΔT_N chosen here is very close to the undercooling, ΔT_c, of a columnar front that would move with the speed of the isotherms. Near the bottom of the ingot, the velocity of the isotherm is large and $\Delta T_c > \Delta T_N$: equiaxed grains thus form. As the velocity decreases, ΔT_c becomes smaller than ΔT_N for case (c) and columnar grains form. However, ΔT_c is still larger than ΔT_N for case (a) and the structure remains equiaxed with a slightly elongated morphology due to the strong thermal gradient. As the superheat is progressively removed, the thermal gradient in the liquid decreases faster and the velocity of the liquidus was shown to increase again. This leads to the formation of elongated and then equiaxed grains above the mid-height of the casting shown in (c). The latent heat released by the equiaxed grains in the upper part of the casting induces a recalescence which stops nucleation and thus leads to the formation of large equiaxed grains.

As can be seen in Fig. 4, the various grain morphologies can be explained in terms of thermal history, grain nucleation and grain growth. The situation is made complex by the variation of both G and v and by the latent heat released by the grains. A simpler situation of constant G and v is shown in **Fig. 5** for an aluminium–silicon alloy of eutectic composition. For the three cases (a)–(c), the thermal gradient, G, and the velocity of the isotherm, v, were fixed to $2 \cdot 10^6$ °C/m and 0.1 m/s, respectively. The length of the solidifying domain (80 μm) corresponds to a temperature range of 160 °C, the eutectic isotherm being precisely located at the top edge at this solidification time. Nucleation of the grains was assumed to occur instantaneously (*i.e.*,

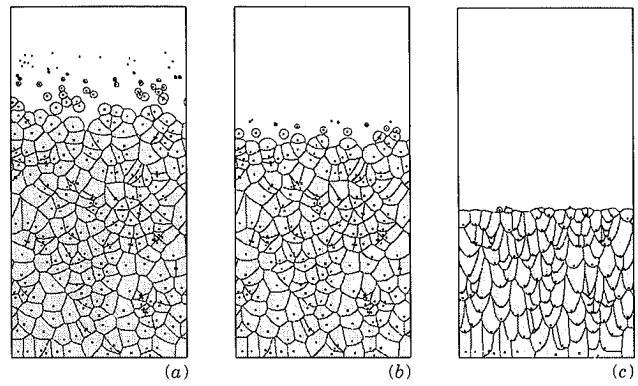

Fig. 5. Two-dimensional simulated grain structures for a eutectic aluminium-silicon alloy solidified at $G = 2 \cdot 10^6$ °C/m and $v = 0.1$ m/s (*i.e.*, cooling rate $\dot{T} = -2 \cdot 10^5$ °C/s). The three cases correspond to various nucleation undercoolings, ΔT_N: 20°C (a), 50°C (b) and 90°C (c). $\Delta T_\sigma = 0$°C and $n_{max} = 1.5 \cdot 10^{16}$ m^{-3}. The three samples have a height of 80 μm and the microstructure is represented when the temperature at the top of the domain is equal to the eutectic temperature.

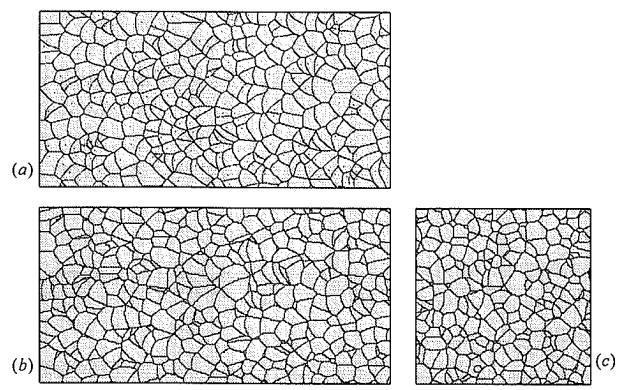

Fig. 6. Comparison of two- (a) and three-dimensional (b, c) grains structures calculated for a eutectic aluminium-silicon alloy solidified in a thermal gradient. The nucleation undercooling and thermal conditions are identical to those of Fig. 5(b). The two micrographs shown at the bottom correspond to a longitudinal (b) and transverse (c) cross sections of the three-dimensional grain structures.

$\Delta T_\sigma = 0$°C) at $\Delta T_N = 20$°C for case (a), $\Delta T_N = 50$°C for case (b) and $\Delta T_N = 90$°C for case (c). The density of grains, n_{max}, was the same in all three cases ($1.5 \cdot 10^{16}$ m^{-3}).

As can be seen in Fig. 5, the "mushy" zone (*i.e.*, the temperature interval over which the grains form) decreases with an increasing value of ΔT_N. At the same time, the asymmetry* of the grains formed in the same thermal gradient increases from (a) to (c). (The centre of nucleation of the grains is delineated by a small dot.) Even though the grains grow faster in the downward heat flow direction (this can be seen in particular in case (a); see also previous section), the final grains after complete solidification are more elongated in the upward direction due to the impingement with previously nucleated grains. The simulated structures of **Fig. 5(b)** can

* The asymmetry of the grains is defined as the ratio of the radius of the grain in the direction of the gradient and that in the opposite direction.

be compared with that shown for the laser-remelted specimen (Fig. 1(b)).

In **Fig. 6**, the final two-dimensional grain structure (a) calculated for the conditions of Fig. 5(b) is compared with a longitudinal section of a three-dimensional simulation shown in (b). The differences are of minor importance and the resulting average asymmetry of the grains is almost identical. This is due to the isotropic nature of the eutectic growth and to the unidirectional heat flow conditions. Such results have been compared to a simple analytical one-dimensional model.[8] The small square shown in **Fig. 6(c)** is a transverse section of the three-dimensional structure (*i.e.*, perpendicular to the travel direction of the laser beam). In this section, the eutectic grains have an equiaxed appearance.

5. Conclusion

Stochastic models describing the nucleation, growth and impingement of grains have been developed for both dendritic and eutectic alloys. These models have been coupled to simple thermal situations or to finite element heat flow computations. The advantages of these models over deterministic models are numerous:

(1) They produce metallographic sections that can be directly compared with experimental micrographs, thus offering a new "computer metallography" tool to materials scientists.

(2) When extended to three dimensions, such simulations allow the actual grain morphology in volume to be related to parameters measured in metallographic sections ("computer stereology").

(3) They can account for both columnar and equiaxed structures. For dendritic alloys, it has been demonstrated that the occurrence of the outer equiaxed zone, of the columnar zone, of elongated and equiaxed grains can be explained by a unique set of nucleation parameters and a single growth kinetics. These different morphologies are then merely dictated by the local thermal conditions (thermal gradient, speed of the isotherms).

(4) The elongated shape of the grains can be explained by such methods. It has been shown that, although the grains grow faster in the downward direction of the heat flow, their final morphology is elongated in the opposite direction due to impingement.

(5) The grain competition that occurs in the columnar zone of dendritic alloys can also be simulated by such methods.[9]

Extensions of these models to three dimensions has already been demonstrated for dendritic alloys.[20,21] The movement or sedimentation of the grains in the liquid has also been simulated for eutectic alloys[22]. At present, the main limitations of such models are the computation cost and the available computer memory space.

Acknowledgments

The authors would like to thank the Commission pour l'Encouragement de la Recherche Scientifique and the Office Fédéral de l'Education et de la Science, Berne, Switzerland, for their financial support (CERS #2361.1 Grant, COST 504 project). They wish also to thank B. Neal for his contribution to the writing of the manuscript.

REFERENCES

1) B. Chalmers: Principles of solidification, John Wiley & Sons, New York, USA, (1964).
2) M. C. Flemings: Solidification Processing, McGraw-Hill, New York, USA, (1974).
3) W. Kurz and D. J. Fisher: Fundamentals of Solidification, Trans. Tech. Pub., Aedermannsdorf, Switzerland, (1989).
4) M. Rappaz: *Int. Mater. Rev.*, **34** (1989), 93.
5) S. G. R. Brown and J. A. Spittle: *Mater. Sci. Technol.*, **5** (1989), 362.
6) M. P. Anderson, D. J. Srolovitz, G. S. Grest and P. S. Sahni: *Acta Metall.*, **32** (1984), 783.
7) P. Zhu and W. Smith: *Acta Metall.*, **40** (1992), 3369.
8) M. Rappaz, Ch. Charbon and R. Sasikumar: *Acta Metall.*, **42** (1994), 2365.
9) Ch.-A. Gandin and M. Rappaz: *Acta Metall.*, **42** (1994), 2233.
10) J. Ampuero, A. F. A. Hoadley and M. Rappaz: Modeling of Casting, Welding and Advanced Solidification Processes, ed. M. Rappaz, M. Ozgu and K. Mahin, T.M.S., Warrendale, Pennsylvania, USA, (1991), 449.
11) T. Sato, W. Kurz and K. Ikawa: *Trans. Jpn. Inst. Met.*, **28** (1987), 1012.
12) W. C. Winegard and B. Chalmers: *Trans. Qt. Am. Soc. Met.*, **46** (1954), 1214.
13) M. Pierantoni, M. Gremaud, P. Magnin, D. Stoll and W. Kurz: *Acta Metall.*, **40** (1992), 1637.
14) W. Kurz, B. Giovanola and R. Trivedi: *Acta Metall.*, **34** (1986), 823.
15) Ch.-A. Gandin, M. Eshelman and R. Trivedi: to be published.
16) K. A. Jackson and J. D. Hunt: *Trans. Am. Inst. Min. Eng.*, **236** (1966), 1129.
17) Ph. Thévoz, M. Rappaz and J.-L. Desbiolles: Light Metals, ed. by Ch. M. Bickert, T. M. S., Warrendale, Pennsylvania, USA, (1990), 975.
18) Th. Imwinkelried and M. Rappaz: Euromat '91, ed. by T. W. Clyne, The Institute of Materials, London, UK, (1992), 191.
19) Ch.-A. Gandin: Modélisation Stochastique de la Solidification: Formation de Structures de Grains Dendritiques, Ph. D. thesis, EPFL, Switzerland, (1994).
20) Ch.-A. Gandin, M. Rappaz and R. Tintillier: *Metall. Trans.*, **24A** (1993), 467.
21) Ch.-A. Gandin, M. Rappaz and R. Tintillier: *Metall. Trans.*, **25A** (1994), 629.
22) Ch. Charbon, A. Jacot and M. Rappaz: *Acta Metall. Mater.*, **42** (1994), 3953.